Sensors and Actuators B 190 (2014) 752–759

Contents lists available at ScienceDirect

Sensors and Actuators B: Chemical

journal homepage: www.elsevier.com/locate/snb

Whispering gallery mode structure and refractometric sensitivity of fluorescent capillary-type sensors

S. Lane, J. Chan, T. Thiessen, A. Meldrum*

Department of Physics, University of Alberta, Edmonton, AB T6G 2E1, Canada

ARTICLE INFO

Article history:
Received 30 July 2013
Received in revised form 3 September 2013
Accepted 4 September 2013
Available online 14 September 2013

Keywords:
Whispering gallery modes
Sensing
Microcapillary
Quantum dots
Microcavity
Sensitivity

ABSTRACT

Fluorescent core microcapillary (FCM) structures present an alternative to optofluidic ring resonators for refractometric or biosensing applications. Instead of a thin-walled capillary that needs to be probed with a tuneable laser, FCMs are comprised of a fluorescent coating deposited on the channel walls of a microcapillary. The high refractive index of the coating serves to confine the fluorescence and leads to the development of whispering gallery modes (WGMs) whose field profile extends into the capillary channel. This work first investigates theoretically the conditions required to optimize the refractometric sensitivity of these structures. The optimal fluorescent coating thickness ultimately represents a trade-off between sensitivity and the mode *Q* factors. We then use a spectral–spatial mapping method to obtain WGM information along the length of a capillary with variable film thickness. The maps agreed well with the theoretical predictions with one main exception: the experimental sensitivities were higher than the predicted values for some modes, possibly owing to interference modulation effects.

1. Introduction

Capillary-based devices have numerous existing and developing sensor applications [1]. In one example, capillaries can be used in microfluidic arrangements to sense local changes of the refractive index of liquid analytes in microfluidic devices [2–5]. In the refractometric mode, a capillary sensor measures only the change in the local index of refraction of the fluid in the channel; whereas in the biosensing mode, the channel surfaces must be chemically pre-treated or functionalized to bind target biomolecules. Many applications have been explored, including disease detection [6], pesticide sensing [7], protein detection [8], and capillary electrophoresis [9]. Furthermore, microcapillary sensors can be compatible with dense, viscous fluids [10]. Capillary-based sensors can be classified into two broad types: liquid-core optical ring resonators (LCORRs) or fluorescent-core microcapillaries (FCMs).

The LCORR, or optofluidic ring resonator, is comprised of a thin-walled glass capillary [4–7,9–11]. Light from a tunable laser is confined by total internal reflection at the interface between the outer wall and the outside air, leading to the development of the cylindrical resonances known as whispering gallery modes (WGMs). Because the walls of the LCORR are thin (*i.e.*, 1–5 μm), a part of the electric field of the WGM extends into the capillary channel, where it can interact with an analyte. This interaction causes a shift of the resonance frequencies, which forms the fundamental sensor transduction mechanism.

In contrast, the FCM makes use of a high-refractive-index fluorescent layer that coats the capillary channel walls (Fig. 1) [5,10,12–14]. The WGMs develop because of the index contrast between the fluorescent layer and the glass wall. In this case a tunable laser is not needed, since the electric field is built up via fluorescence in the coating, which can be excited with a diode laser or LED. These devices are robust, but it is difficult to control the thickness of the coating [5,14], which can affect the sensitivity of the structure to analytes pumped into the channel region. Thus, an objective of the present work was to perform a theoretical and experimental analysis of the effects of the fluorescent coating thickness on the sensitivity of the FCM structure. This can determine the geometries (*e.g.*, film thickness and capillary diameter) required for optimal sensing performance.

2. Materials and methods

Microcapillaries with a fluorescent quantum dot layer coating the channel were prepared using methods previously described [15]. Briefly, capillaries from Polymicro Technology with a nominally 30 ± 2 μm inner diameter were first heated for 45 min at 650 °C in flowing O_2 to ash the polyamide jacket. Next, the capillaries were filled with a solution of hydrogen silsesquioxane (HSQ) dissolved in methyl isobutyl ketone (MIBK). The capillaries were

Abbreviations: WGM, whispering gallery mode; FCM, fluorescent core microcapillary; *Q* factor, quality factor.

* Corresponding author. Tel.: +1 780 492 5342.
E-mail address: ameldrum@ualberta.ca (A. Meldrum).

0925-4005/$ – see front matter © 2013 Elsevier B.V. All rights reserved.
http://dx.doi.org/10.1016/j.snb.2013.09.029

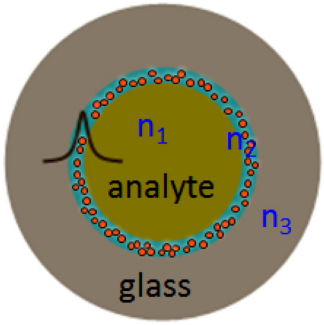

Fig. 1. Cross sectional diagram of the FCM structure, which consists of a high-index fluorescent layer (n_2) coated onto the channel wall of a glass capillary (n_3). The analyte (n_1) flows within the channel. The electric field profile of a WGM resonance is represented schematically by the black line.

then annealed in a two-step procedure: 3 h at 300 °C to evaporate the MIBK, and a subsequent hour at 1100 °C to cause the remaining HSQ to separate into a coating consisting of fluorescent silicon quantum dots embedded in a silica film. Some of the fluorescent capillaries formed with this method contain films that have varying thickness along the length of the capillary. A single capillary showing considerable variation in film thickness along its length was chosen for these experiments.

An approximately 4-cm-long capillary was supported such that it extended over a microscope objective. The ends of the capillary were glued to Teflon tubing (using Norland #76 adhesive) and a syringe pump was used to inject fluids into the tube. The fluorescence was excited using a 445-nm diode laser incident on the capillary via free space, focused to a spot size on the capillary of several hundred μm^2. The fluorescence was collected through the objective (Fig. 2) and sent to an SGS imaging spectrometer from the Santa Barbara Instruments Group. In this instrument, first optic is a mirror with a 100-μm entrance slit located in the center. One camera (the "tracking CCD") is aligned to accept images reflected from the mirror (which will contain a dark image of the slit superimposed on the microscope image). Light that passes through the slit enters the spectrograph part of the instrument and the spectrum is recorded by a second imaging CCD.

The capillary was carefully rotated so that its axis would be parallel to the spectrometer entrance slit, as observed on the tracking image (see Fig. 2). This orientation permits a spectral map to be obtained along the length of the capillary; the resulting spectral map has wavelength on the horizontal axis and distance (parallel to the capillary length) on the vertical one. Initially, the capillary tended to settle or drift slightly in its mounting, a tendency that caused some difficulty in obtaining data from the identical region of the capillary over long time periods. This behavior was minimized by mounting the capillary firmly using a low-melting-temperature wax and waiting for several hours before starting data collection.

In order to measure the refractometric sensitivity, deionized water and then ethanol were pumped into the channel while fluorescence spectra were being collected. The collection time was 20 s per spectrum. Dispersion effects are quite small over the wavelength range of 790–850 nm over which the spectra were collected, so we used fixed values of $n_{water} = 1.329$ and $n_{ethanol} = 1.357$ to estimate the experimental sensitivity. All spectra were calibrated for wavelength and intensity, by using an HgAr calibration lamp and a blackbody source (the LS1 from Ocean Optics), respectively.

3. Basic theory

We use the work of Teraoka and Arnold [16,17] as the starting point for understanding layered capillary structures. Their work showed how the refractometric sensitivity of a layered sphere can be controlled by film thickness. One of the most interesting results was that there was an optimal film thickness at which the sensitivity of a layered microsphere reaches a maximum. Essentially, when the high-index coating is very thin, it tends to "pull" the electric field from the inside toward the sphere surface and allows a greater fraction to extend outward into the analyte, increasing the sensitivity. However, as the high-index layer is made thicker, the evanescent field in the analyte also begins to contract inward toward the film and the sensitivity is reduced. Lin et al. subsequently extended the work toward a sensitivity and temperature analysis of the LCORR structure [18], and Franchimon et al. examined the WGM frequency shifts induced by nearby waveguides or fiber tapers [19].

Here, we follow the work of Teraoka and Arnold [16,17], extending it toward capillary structures with an absorbing layer. Accordingly, for a capillary with a single channel layer, the electric field profile can be written as:

$$E_z(r) = Z \begin{cases} AJ_l(n_1 k_0 r), & r \le a - t \\ BH_l^2(n_2 k_0 r) + CH_l^1(n_2 k_0 r), & a - t < r \le a \\ DH_l^1(n_3 k_0 r), & r > a \end{cases} \quad (1)$$

where a is the inner radius of the capillary, t is the film thickness, and Z is a proportionality constant. Applying the appropriate boundary conditions leads to the following two equations for the transverse electric (TE) and transverse magnetic (TM) polarizations:

$$\text{TE}: \frac{n_3 H_l^{1'}(n_3 k_0 a)}{n_2 H_l^1(n_3 k_0 a)} = \frac{(B_l/C_l) H_l^{2'}(n_2 k_0 a) + H_l^{1'}(n_2 k_0 a)}{(B_l/C_l) H_l^2(n_2 k_0 a) + H_l^1(n_2 k_0 a)} \quad (2)$$

$$\text{TM}: \frac{n_2 H_l^{1'}(n_3 k_0 a)}{n_3 H_l^1(n_3 k_0 a)} = \frac{(B_l/C_l) H_l^{2'}(n_2 k_0 a) + H_l^{1'}(n_2 k_0 a)}{(B_l/C_l) H_l^2(n_2 k_0 a) + H_l^1(n_2 k_0 a)} \quad (3)$$

In Eqs. (1)–(3), J_l and $H_l^{1,2}$ are the cylindrical Bessel and Hankel functions of order l, where l is the angular mode number of the WGM, defining the number of wavelengths that "fit" around the capillary circumference. The prime indicates the radial derivative

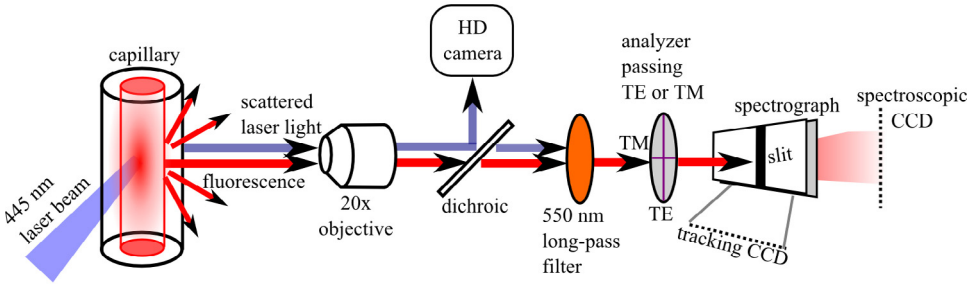

Fig. 2. Diagram illustrating the experimental setup.

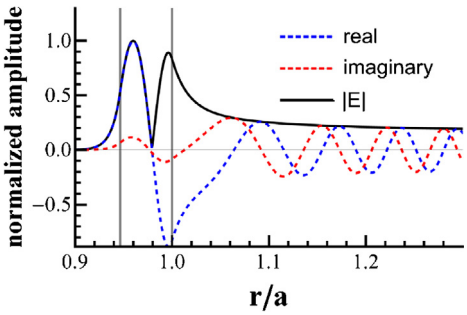

Fig. 3. Electric field amplitude profile of a second-order mode ($n = 2, l = 195$, TE polarization) of a capillary with a radius of 15 μm and a film thickness of 0.8 μm. The coating is bounded by the vertical gray lines. This is an example of a low-Q mode ($Q = 430$), as evidenced by the large evanescent extension.

of the function, as usual. The polarizations are defined with respect to the WGM plane, so that E (TE) and H (TM) are parallel to the capillary axis. The ratios B_l/C_l are given by:

$$\left(\frac{B_l}{C_l}\right)_{TE} = \frac{n_2 J_l(n_1 k_0 z) H_l^{1'}(n_2 kz) - n_1 J_l'(n_1 k_0 z) H_l^1(n_2 k_0 z)}{-n_2 J_l(n_1 k_0 z) H_l^{2'}(n_2 kz) + n_1 J_l'(n_1 k_0 z) H_l^2(n_2 k_0 z)} \quad (4)$$

$$\left(\frac{B_l}{C_l}\right)_{TM} = \frac{n_1 J_l(n_1 k_0 z) H_l^{1'}(n_2 kz) - n_2 J_l'(n_1 k_0 z) H_l^1(n_2 k_0 z)}{-n_1 J_l(n_1 k_0 z)) H_l^{2'}(n_2 kz) + n_2 J_l'(n_1 k_0 z) H_l^2(n_2 k_0 z)} \quad (5)$$

Eqs. (2) and (3) have an infinite number of roots, k_0, corresponding to the radial mode orders with complex wavevectors $k_{0,1}$, $k_{0,2}$, $k_{0,3}$ . . .. Here, we will only examine the three lowest-order solutions corresponding to the cases where 1–3 intensity maxima extend in the radial direction. An example result is shown in Fig. 3, in which the field profile is shown for an $n = 2$ mode. As we will show below, the first-order solutions are the dominant ones experimentally in FCM structures; for $n \geq 2$, the modes tend to be lossy and usually do not appear in experiment.

We will assume that the capillary wall is lossless, but examine the effects of absorption-related losses in the fluorescent layer and in the analyte, by numerically finding the complex roots of Eqs. (2) and (3). The solutions give a resonance wavelength ($\lambda_0 = 2\pi/Re[k]$) and Q-factor ($Q = Re[k]/2Im[k]$), as is well known (*e.g.*, Ref. [18]). The refractometric sensitivity $d\lambda/dn_1$ can be calculated by integration [17,18], although in an FCM structure the relatively low index contrast between the film and the glass wall can lead to open resonator issues with the integration limits, similar in a sense to the case for mode volume calculations [20]. Here, we simply find the solutions to Eqs. (2) and (3) over a narrow range of refractive index in the core, and calculate $\Delta\lambda/\Delta n_1$ over this range. This method is reasonably accurate, as the sensitivity is virtually constant over a narrow range of n_1.

The detection limit, D, depends on the sensitivity and the resolution, R, of the spectrometer system: $D = R/S$, in refractive index units. R is the minimum WGM wavelength shift detectable by the spectrometer, typically within a 3σ level of certainty. A high Q factor was generally thought necessary for a good resolution [21]; however, a complete consideration showed that high Q factors are not strictly necessary, especially if the resonances are periodic [22]. An important question here is to determine whether there is an optimal fluorescent coating thickness for the case of a capillary structure.

4. Results and discussion

4.1. WGM field calculations

The calculated electric field profiles for the first-order radial modes are shown as a function of film thickness in Fig. 4. The layer

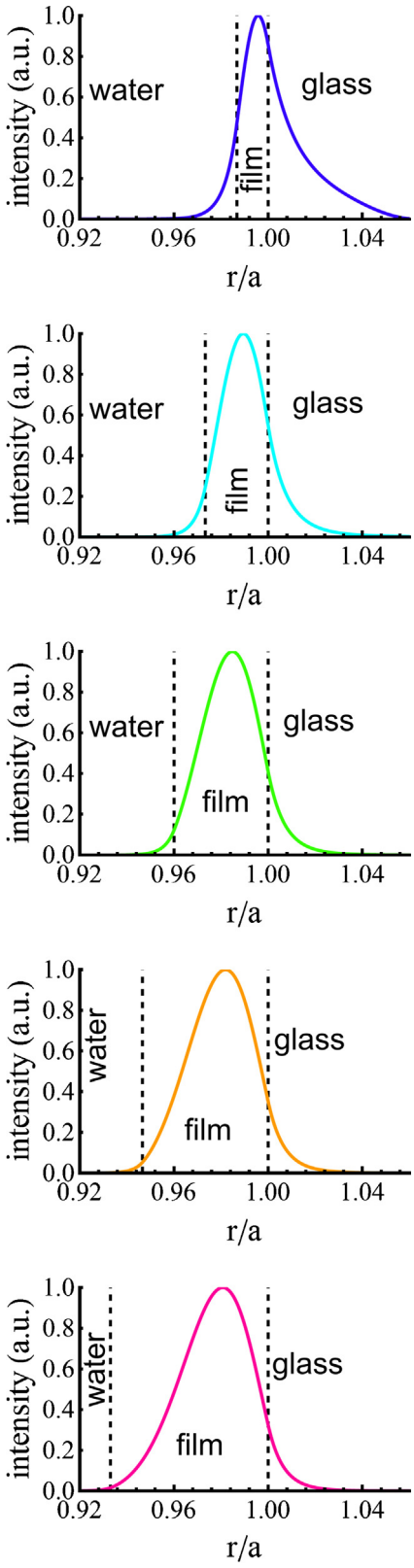

Fig. 4. First-order mode profiles (angular mode number $l = 195$) for different film thicknesses, for a glass ($n_3 = 1.45$) capillary of inner radius 15 μm, with water in the channel ($n_1 = 1.33$). The coating thicknesses correspond to 0.2, 0.4, 0.6, 0.8, and 1.0 μm, and the refractive index is 1.67. The resonance wavelength for these modes is close to 770 nm.

index was assumed to be 1.67, in agreement with ellipsometry results for a flat quantum-dot film made by similar methods [5]. For the thinnest films, much of the mode extends into the glass capillary, although a fraction remains in the analyte. As the film becomes thicker, the mode is "concentrated" into the film region from both sides. The TM mode profiles (not shown) evolved similarly.

When the fluorescent film is very thin, increasing its thickness leads to a nearly exponential increase in the radiation-limited Q factor (Fig. 5(b)), similar to what happens for microspheres [23], as well as a decrease in the sensitivity (Fig. 5(c)). However, as the film becomes thicker, the Q factor tends to saturate. Once the mode field profile is completely inside the coating there is little further effect to increasing the thickness. The sensitivity of the first-order modes in FCM structures decreases monotonically over the calculated range of t (Fig. 5(c)). For film thicknesses below ~0.2 μm, the Q factor becomes extremely low (*i.e.*, <100), and for such thin coatings the finesse is so low that the FCMs may be impractical for refractometric sensing. Calculations also showed that the TM-polarized modes are more sensitive to refractive index changes in the analyte than are the TE-polarized ones, and have slightly lower Q factors.

In the case of thin-walled LCORRs, the higher-order radial modes present an excellent option for improving the sensitivity [10,24]. For the FCM structures investigated here, the situation is somewhat different. Essentially, the higher index of the wall material (compared to air in the case of LCORRs) gives the second-order radial modes a larger amplitude in the glass capillary wall (Fig. 6), similar to the behavior of an evanescent field of a bound waveguide mode. This implies that these modes will be much lossier than the first-order case. Thus, although the second-order modes do extend farther into the analyte for a 1-μm-thick film, the field profiles suggest that they are only weakly confining and would thus be difficult to observe in a fluorescence spectrum – in other words, FCMs are "single moded" [14], at least as long as the channel fluid index is not too high [10]. Furthermore, unlike the LCORR, in which a significant fraction of the field can extend into the analyte if the capillary walls are very thin, a relatively smaller fraction of the field extends into the FCM channel region for all coating thicknesses (essentially the WGM field profile is skewed in a manner that depends on the refractive indices of the three layers).

The Q factors and sensitivities of the first three radial modes are compared in Fig. 7. The higher-order radial modes always have a greater sensitivity, although the Q factors are orders of magnitude smaller. Thus, despite the higher sensitivity, the $n = 2,3$ modes will probably not be observable in a typical fluorescence spectrum, with a relatively low-index fluid such as water or ethanol in the capillary channel.

Fluorescent coatings may have non-negligible absorption at the emission wavelengths. In the case of the Si–QD films used in this work, the extinction coefficient was measured by ellipsometry to be $\kappa = 0.0006$ at wavelengths near 800 nm. While the structure of a flat QD film may be slightly different than it would be in a capillary, we assumed this value for the channel coating. Absorption losses do not significantly affect the resonance wavelength or the sensitivity, but they do of course limit the ultimate Q factor achievable in an FCM device (Fig. 8). For $\kappa = 6 \times 10^{-4}$, the Q factor for both polarizations saturates at around 1500 when the film thickness reaches approximately 300 nm (TE) or 400 nm (TM). This result will be compared with the experimental values shortly.

The effect of analyte absorption on the WGMs may offer an alternative transduction mechanism for sensing [25]. The total Q factor is simply given by $1/Q_{total} = 1/Q_{rad} + 1/Q_{abs} + ...$, where Q_{rad} is the radiation limited Q factor and Q_{abs} incorporates material-related losses such as absorption. Thus, material losses can be a dominant effect for some structures, especially for an FCM where

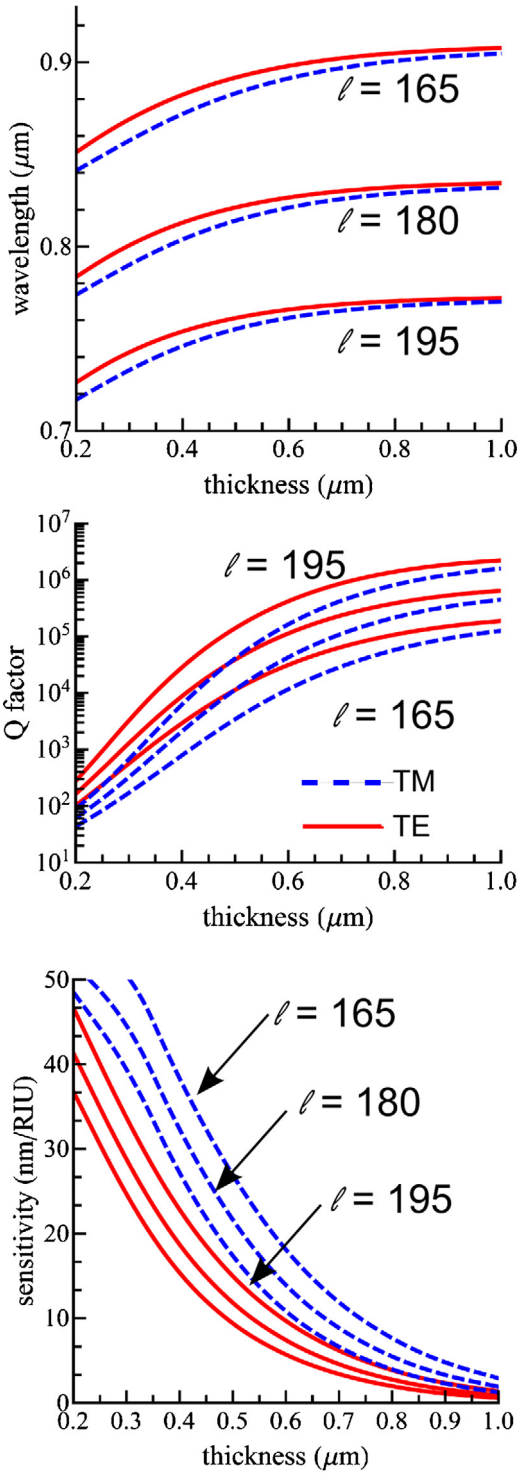

Fig. 5. Resonance wavelength, Q factor, and sensitivity for the first-order $l = 165$, 180, and 195 WGMs, as a function of layer thickness. In the center plot, the $l = 180$ mode occurs between the other two, but is not labeled. Solid red lines indicate TE, and dashed blue lines indicate TM polarization.

the fluorescent layer is absorbing. In order to investigate this further, the Q factors were calculated as a function of film thickness, for different values of the analyte extinction coefficient (Fig. 9). There are essentially three regimes, which depend on coating thickness. For coatings thinner than 300–400 nm, the Q factors increase almost exponentially. In this regime, increasing the coating thickness greatly enhances modal confinement and reduces the fraction

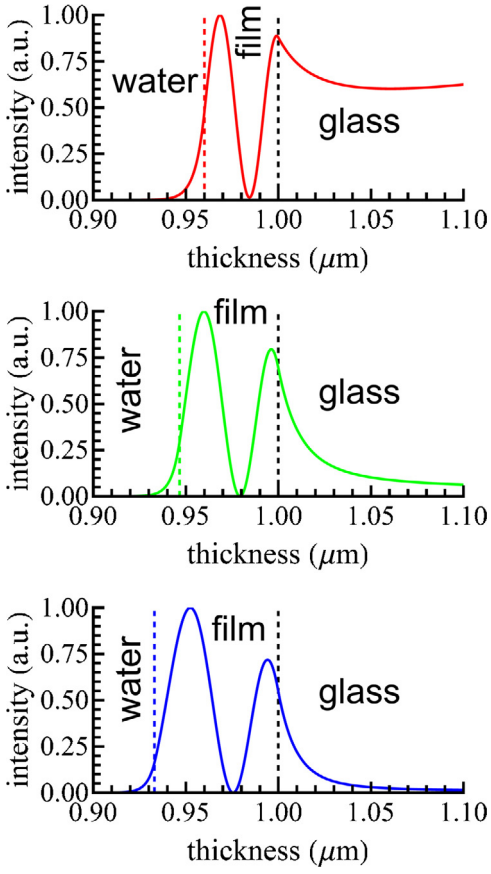

Fig. 6. Second-order mode profiles (angular mode number $l = 195$) for different film thicknesses, for a glass ($n_3 = 1.45$) capillary of inner radius 15 μm, with water in the channel. The coating thicknesses are 0.6, 0.8, and 1.0 μm and the refractive index is 1.67. The peak wavelength for these modes is close to 705 nm. For the 600 μm film, the Q factor is only ~60.

of the mode within the absorbing analyte. In the second regime, for coating thicknesses between about 0.4 and 1.5 μm, the Q factors increase at a slower rate. In this regime, the main effect of increasing coating thickness is to decrease exposure of the mode field to the absorbing analyte. Finally, at a thickness about ~1.5 μm, the effect of further thickening the coating becomes negligible, since there is essentially no longer any extension of the mode field into the analyte.

Of course, a real sample may have absorption both in the fluorescent coating and in the analyte. In that case, the effect of analyte absorption is smaller (in terms of a change in the Q factor). Thus, using the change in Q due to analyte absorption as a sensing mechanism in FCMs would likely be difficult to achieve, requiring thin coatings and/or very low absorption in the QD layer.

4.2. Comparison with experiment

A representative capillary and the corresponding TM polarized WGM spectrum is shown in Fig. 10. The QD film appears as a bright line along the channel walls. Tracking a single bright band vertically along the image shows how that particular mode shifts in wavelength along the capillary due to changes in the film thickness. In the thicker-coating regions, the spectral map shows more detailed, patterned mode structure (Fig. 10, inset).

The WGMs are clear and well-formed in both polarizations, and are characterized by a free spectral range (FSR) of 3.6–4.0 nm, a visibility up to 0.4, and a finesse as high as 8.0 (Fig. 11). The modes tend

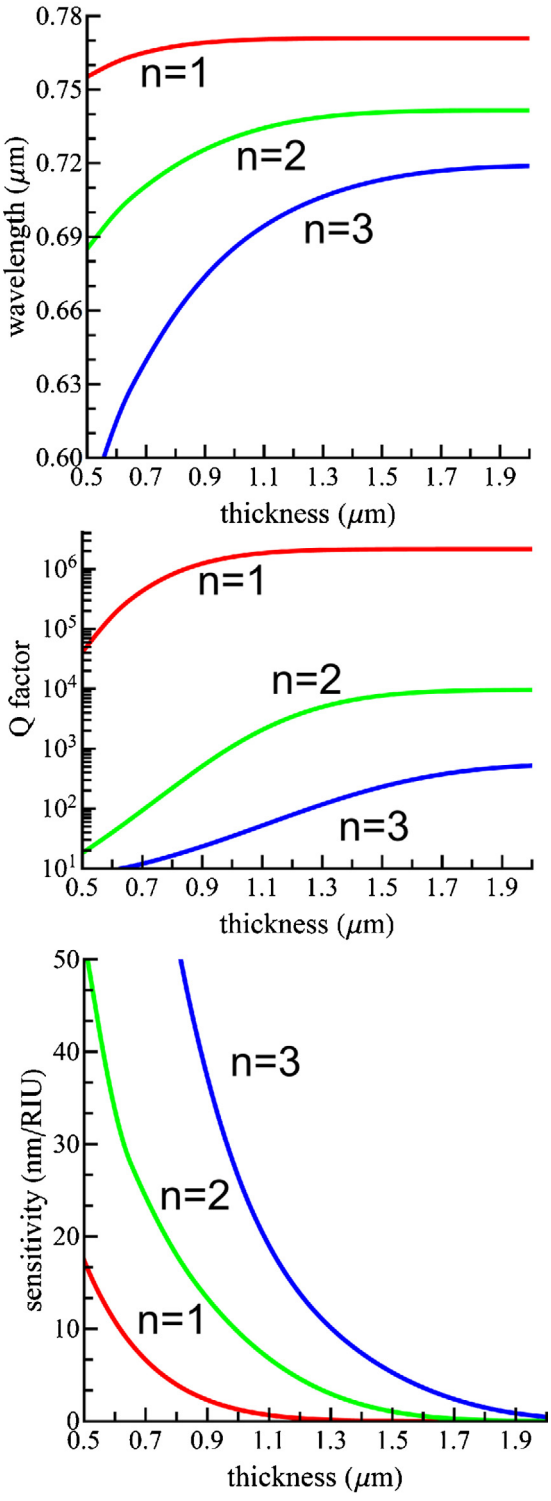

Fig. 7. A comparison of the resonance wavelength, Q factor, and sensitivity for the first three radial orders ($l = 195$, TM polarization).

to be highly asymmetrical and are skewed to shorter wavelengths. Thus, in order to estimate the resonance wavelengths, individual WGMs were cropped from the spectrum and fit with a modified skewed Lorentzian function [22,26] given by

$$P(\lambda) = \frac{2A/\pi\gamma(\lambda)}{[1 + 4(\lambda - \lambda_0/\gamma(\lambda))^2]} \quad (6)$$

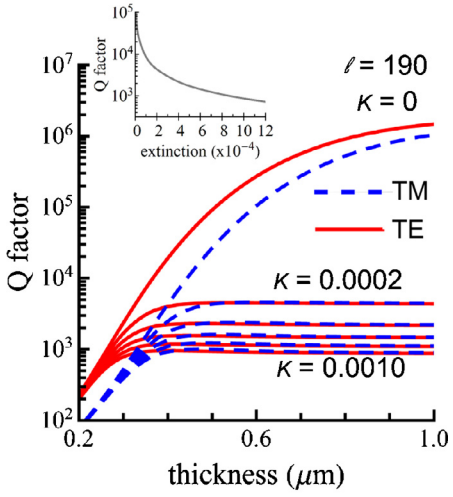

Fig. 8. Resonance Q factor for the first-order $l = 190$ WGM, as a function of absorbing layer thickness. The extinction coefficient steps in units of 0.0002. Solid red lines indicate TE, and dashed blue lines indicate TM polarization. The inset shows the Q-factor at saturation, as a function of extinction coefficient for a 2 μm thick coating.

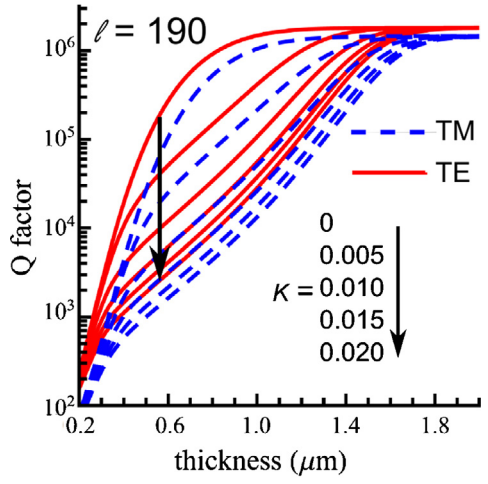

Fig. 9. Resonance Q factor for the first-order $l = 190$ WGM, as a function of analyte absorption. Solid red lines indicate TE, and dashed blue lines indicate TM polarization.

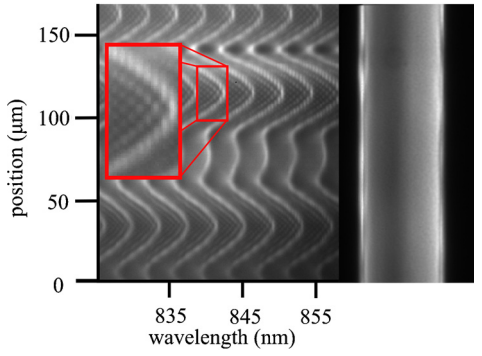

Fig. 10. Fluorescence spatial–spectral map (left) of a section of microcapillary and its corresponding TM spectrum. The inset shows finer mode structure in the thick region. The right side shows a fluorescence image of the capillary channel with the position scale approximately aligned to the spectral map.

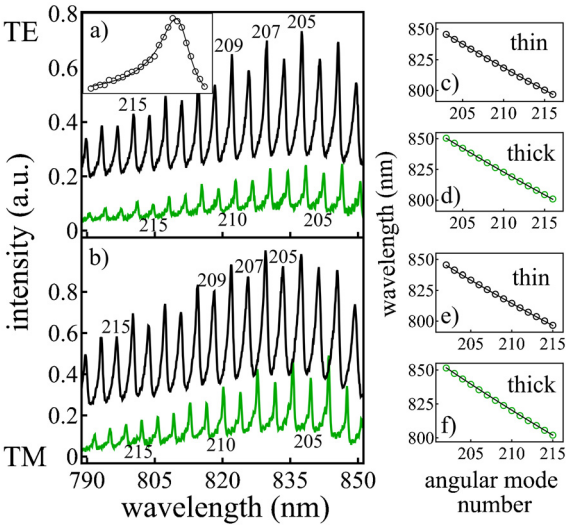

Fig. 11. TE (a) and TM (b) polarized fluorescence spectra for thin (black lines) and thick (green lines) films on the microcapillary, with water in the channel. Data is offset for clarity. The inset in (a) shows the experimental $l = 206$ TM mode for the thin film on the microcapillary fit with the modified skewed Lorentzian function (Eq. (6)). The sidebar (c–f) illustrates the agreement between experiment (data points) and theory (line) for films with a thickness of 695 nm (thin) and 930 nm (thick).

Here, λ_0 is the central wavelength, A is a normalizing factor, and the peak width γ describes the wavelength-dependence width:

$$\gamma(\lambda) = \frac{(1+B)\gamma_0}{1 + Be^{a(\lambda-\lambda_0)}} \tag{7}$$

Eq. (6) provides an excellent fit to the data (see Fig. 11(a), inset) and permits one to find the peak position more accurately than simply by visual estimation, although this equation does not have a specific physical meaning with respect to the WGMs.

The film thickness at any location in the capillary was estimated by modeling the peak positions of the experimental WGM spectra using Eqs. (2) and (3), and solving for the capillary radius and film thickness that matched the experimental observations. The results are shown in the sidebar of Fig. 11, for two regions of the FCM with water in the channel. The agreement between theory and experiment is excellent for coating thicknesses of 695 nm (thin region) and 930 nm (thick region), for both polarizations and for both fluids in the channel (water and ethanol), with a capillary radius of 17.2 μm, which is close to but somewhat outside the nominally 15 ± 1 μm radius of these capillaries according to the manufacturer [27].

The mode skewing is due to a set of spiraling modes traveling with a component of the wavevector along the capillary axis [28,29]. The data show that for thinner films, the WGMs are broadly skewed to shorter wavelengths, but no individual spiraling modes can be observed. For thicker films, the spiraling modes become better resolved into a set of small peaks on the short-wavelength side of the main one (Fig. 12). These modes are not simply higher-order radial modes, since they do not follow the expected spectral positions, Q factors, or sensitivity for different fluids in the capillary channel (instead, they simply tend to closely follow the main WGM). Similar spiral mode effects have been seen previously in an LCORR structure [3], in which the spiral modes were sometimes resolvable (similar to Fig. 12: thick film) or otherwise appeared as a broad, short-wavelength skewing, more like the thin-coating spectra presented here. This skewing makes the measured Q factors for the peaks shown in Fig. 12 lower than the theoretical ones for thinner coatings. When the main WGM becomes clearly separate from the adjacent set of spiral modes, however, the Q factor was measured to be ~1450. This is in close

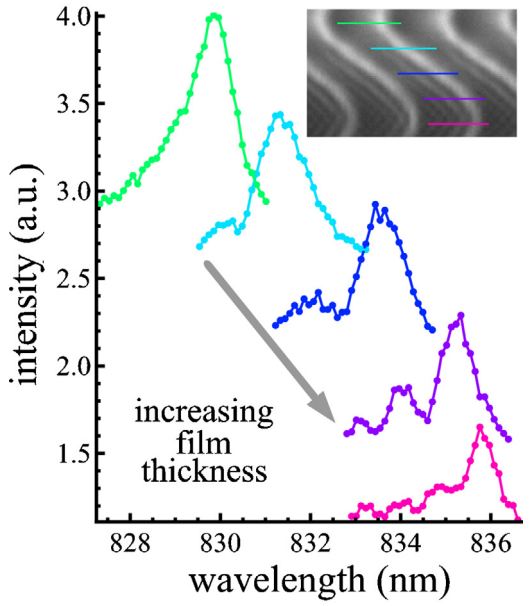

Fig. 12. The experimental $l = 206$ TM mode for different coating thicknesses. The data has been offset for clarity. The top inset shows the spectral map from which the measurements were taken, with the line profiles color-coded to match the main spectra. The WGM Q factor appears to increase as the skew modes become increasingly well resolved for the thicker-coatings.

agreement with the theoretical value shown in Fig. 8 for a film with $\kappa = 6 \times 10^{-4}$ (keeping in mind that the calculations described earlier do not model wave propagation along the cylinder axis).

The experimental and theoretical sensitivities are shown for two different film thicknesses in Fig. 13. The TM modes were always more sensitive, in agreement with theory. One surprising result in the experimental data is the appearance of an oscillation in the sensitivity of adjacent angular modes in some cases (this is especially noticeable for the "TM thin" data set). One set of alternating angular modes has sensitivities that agree well with theory, while the other set is much more sensitive. Similar effects were observed to some degree in several of the other spectra as well. In some cases, the alternating sensitivity pattern is not observable (*i.e.*, TE thick) but all of the modes are more sensitive than expected.

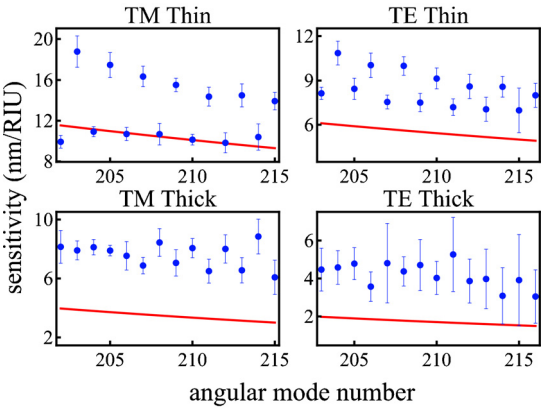

Fig. 13. Measured (blue) and calculated (red) sensitivities as a function of angular mode number, for FCMs with a thin (695 nm) or thick (930 nm) QD coating. Note the variation in the sensitivities of alternating angular modes that is especially apparent in the thin film TM case. The theoretical sensitivity closely matches the lower-sensitivity group of modes. In the other cases, this alternating behavior is not as clear, and but all the modes are more sensitive to changes in the core index than would be predicted by theory. Error bars were calculated from the uncertainty in the peak fitting procedure for each WGM.

While a full study of the enhanced sensitivity effect is outside the scope of this work, we hypothesize that the periodic oscillations observed in Fig. 13 (which, in fact, correspond with intensity oscillations in some spectra in Fig. 11) can arise from an interference modulation effect. Fabry–Perot (F–P) type resonances in the film [30] could couple to the WGMs, but can be ruled out on account of the very large FSR for F–P resonances in the QD coating. Interior resonances of the capillary channel could also couple to the main WGMs, but these would have very low Q factors associated with lossy external reflections at the channel-coating interface. On the other hand, outer "wall interferences" similar to those reported in Ref. [31] could be important in the present case also.

Capillary wall interferences are caused by external reflection of a portion of the emitted fluorescence at the interface between the capillary wall and the outside air. Knight et al. [31] used a simple ray picture to describe the condition required for the wall reflections to interfere constructively with the core WGMs. Following their method, we find that there is nearly a 5:2 ratio for the resonance periods of the wall reflections and the core WGMs, respectively, for an outer capillary radius of 156 μm, in close agreement with the thickness measured for the same capillary with the jacket removed. This suggests the possibility that interference from wall reflections could cause the modulations observed in the peaks heights and sensitivity for alternating WGMs.

A complete investigation of this effect is outside the scope of the present work; here, we simply find that whenever a WGM moves from constructive to destructive interference with the calculated wall reflections (or vice versa) when the analyte in the channel changes, the sensitivity is higher than predicted for that mode. Analysis of the WGM spectra showed that this occurred for all the resonances in the thick film case ("high" peaks changed to "low" peaks, and vice versa, on changing from water to ethanol in the channel) so they are all "too sensitive", but for only one set of alternating angular resonances in the thin film case. If correct, this hypothesis implies that, by optimizing the capillary wall radius for a given structure, these interference modulations could in principle be used to improve the sensitivity of FCM structures beyond the values predicted from Eqs. (2) and (3).

5. Conclusion

In the first part of this work, we mapped the predicted behavior of the wavelength, Q factor, and sensitivity over a wide range of coating thicknesses, for FCM-type refractometric sensors. Unlike the case for a microsphere, these structures have no optimum coating thickness required to achieve the highest sensitivity. Instead, thinner films are always better, at least until the Q factor degrades to the point at which the WGMs become difficult to resolve. The TM-polarized WGMs are also predicted to always have a higher sensitivity than the TE case. For thicker coatings, the Q factors saturate at values depending on the losses in the fluorescent film. These results were in agreement with experiment, for an FCM in which silicon QDs were used as the high-index fluorescent coating layer.

By imaging the luminescence spectrum along the length of a capillary, a complete map of WGM spectral information can be obtained as a function of varying QD-coating thickness along the capillary length. This method can permit more information to be obtained than does the method used previously [5,10], but it was found to be very sensitive to sample drift. The WGM spatial–spectra map showed considerable structure, featuring the development of spiraling modes that appeared on the short-wavelength tail of the main WGMs. These modes were always better resolved when the coating was thicker. Finally, many of the individual WGMs were more sensitive than predicted theoretically, reaching values of ~20 nm/RIU for the first-order TM WGMs for a coating thickness

of 695 nm. This could be due to an interference modulation associated with external reflections at the outer capillary wall. Coupling between core WGMs and wall interferences could be used in future to help improve the FCM sensitivity beyond the predicted limits for these devices.

Acknowledgements

The authors thank and acknowledge the NSERC Discovery and the AITF iCiNano programs for funding support, and the Veinot group for access to materials. Thanks to Ray DeCorby for a discussion on the capillary wall interferences.

References

[1] M. Borecki, M.L. Korwin-Pawlowski, M. Beblowska, J. Szmidt, A. Jakubowski, Optoelectronic capillary sensors in microfluidic and point-of-care instrumentation, Sensors 10 (2010) 3771–3797.
[2] I.M. White, H. Zhu, J.D. Suter, N.M. Hanumegowda, H. Oveys, M. Zourob, X. Fan, Refractometric sensors for lab-on-a-chip based on optical ring resonators, IEEE Sensors Journal 7 (2007) 28–35.
[3] V. Zamora, A. Díez, M.V. Andrés, B. Gimeno, Refractometric sensor based on whispering gallery modes of thin capillaries, Optics Express 15 (2007) 12011–12016.
[4] I.M. White, H. Oveys, X. Fan, Liquid-core optical ring-resonator sensors, Optics Letters 9 (2006) 1319–1321.
[5] C.P.K. Manchee, V. Zamora, J. Silverstone, J.G.C. Veinot, A. Meldrum, Refractometric sensing with fluorescent-core microcapillaries, Optics Express 19 (2011) 21540–21551.
[6] J.T. Gohring, P.S. Dale, X. Fan, Detection of HER2 breast cancer biomarker using the opto-fluidic ring resonator biosensor, Sensors and Actuators B: Chemical 146 (2010) 226–230.
[7] G. Yang, I.M. White, X. Fan, An opto-fluidic ring resonator biosensor for the detection of organophosphorus pesticides, Sensors and Actuators B: Chemical 133 (2008) 105–112.
[8] F. Vollmer, D. Braun, A. Libchaber, M. Khoshsima, I. Teraoka, S. Arnold, Protein detection by optical shift of a resonant microcavity, Applied Physics Letters 80 (2002) 4057–4059.
[9] H. Zhu, I.M. White, J.D. Suter, M. Zourob, X. Fan, Integrated refractive index optical ring resonator detector for capillary electrophoresis, Analytical Chemistry 79 (2007) 930–937.
[10] V. Zamora, Z. Zhang, A. Meldrum, Refractometric sensing of heavy oils in fluorescent core microcapillaries, Oil Gas Science and Technology (2013), http://dx.doi.org/10.2516/ogst/2013113 (in press).
[11] K. Scholten, X. Fan, E.T. Zellers, Microfabricated optofluidic ring resonator structures, Applied Physics Letters 99 (2011) 141108.
[12] G. Huang, V.A. Bolanos Quinones, F. Ding, S. Kiravittaya, Y. Mei, O.G. Schmidt, Rolled-up optical microcavities with subwavelength wall thicknesses for enhanced liquid sensing applications, ACS Nano 4 (2010) 3123–3130.
[13] P. Bianucci, J.R. Rodriguez, C. Clements, C.M. Hessel, J.G.C. Veinot, A. Meldrum, Whispering gallery modes in silicon nanocrystal coated microcavities, Physica Status Solidi A 206 (2009) 965.
[14] K.J. Rowland, A. François, P. Hoffman, T. Monro, Fluorescent polymer coated capillaries as optofluidic refractometric sensors, Optics Express 21 (2013) 11492–11505.
[15] S. McFarlane, C.P.K. Manchee, J.W. Silverstone, J.G.C. Veinot, A. Meldrum, Synthesis and operation of fluorescent-core microcavities for refractometric sensing, Journal of Visualized Experiments 73 (2013) e50256.
[16] I. Teraoka, S. Arnold, F. Vollmer, Perturbation approach to resonance shifts of whispering-gallery modes in a dielectric microsphere as a probe of a surrounding medium, Journal of the Optical Society of America B 20 (2003) 1937–1946.
[17] I. Teraoka, S. Arnold, Enhancing sensitivity of a whispering gallery mode microsphere sensor by a high-refractive index surface layer, Journal of the Optical Society of America B 23 (2006) 1434–1441.
[18] N. Lin, L. Jiang, S. Wang, H. Xiao, Y. Lu, H.-L. Tsai, Applied Optics 50 (2011) 3615–3621.
[19] E.F. Franchimon, K.R. Hiremath, R. Stoffer, M. Hammer, Journal of the Optical Society of America B 30 (2013) 1048–1067.
[20] I.H. Agha, J.E. Sharping, M.A. Foster, A.L. Gaeta, Optimal sizes of silica microspheres for linear and nonlinear optical interactions, Applied Physics B: Lasers 83 (2006) 303–309.
[21] I.M. White, X. Fan, On the performance quantification of resonant refractive index sensors, Optics Express 16 (2008) 1020–1028.
[22] J.W. Silverstone, S. McFarlane, C.P.K. Manchee, A. Meldrum, Ultimate resolution for refractometric sensing with whispering gallery mode microcavities, Optics Express 20 (2012) 8284–8295.
[23] L.A. Weinstein, Open Resonators and Open Waveguides, The Golem Press, Boulder, CO, 1969.
[24] H. Li, X. Fan, Characterization of sensing capability of optofluidic ring resonator biosensors, Applied Physics Letters 97 (2010) 011105.
[25] T. Ling, L.J. Guo, Analysis of the sensing properties of silica microtube resonators, Journal of the Optical Society of America B 26 (2009) 471–477.
[26] A.L. Stancik, E.B. Brauns, A simple asymmetric line shape for fitting infrared absorption spectra, Vibrational Spectroscopy 47 (2008) 66–69.
[27] http://www.polymicro.com/mx_upload/superfamily/polymicro/pdfs/capillarytubing_tsp_tsg.pdf
[28] A.W. Poon, R.K. Chang, Spiral morphology-dependent resonances in an optical fiber: effects of fiber tilt and focused Gaussian beam illumination, Optics Letters 23 (1998) 1105–1107.
[29] V. Zamora, A. Diez, M.V. Andrés, B. Gimeno, Interrogation of whispering-gallery modes resonances in cylindrical microcavities by backreflection detection, Optics Letters 34 (2009) 1039–1041.
[30] A. Mazhorova, A. Markov, B. Ung, M. Rozé, S. Gorgutsa, M. Skorobogatiy, Thin chalcogenide capillaries as efficient waveguides from mid-infrared to terahertz, Journal of the Optical Society of America B 29 (2012) 2116–2123.
[31] J.C. Knight, H.S.T. Driver, G.N. Robertson, Interference modulation of Q values in a cladded-fiber whispering-gallery-mode laser, Optics Letters 18 (1993) 1296–1298.

Biographies

Stephen Lane received a BSc in physics from the University of Calgary in 2012. He is currently a Masters student in condensed matter physics at the University of Alberta. Stephen is also a Grade-I bagpiper in his spare time.

Judy Chan is currently pursuing a BSc in Nanoscience at the University of Guelph. She is interested in biosensing devices and applications relevant to the biomedical and food processing industries, and is currently a summer intern at the University of Alberta.

Torrey Thiessen is beginning his fourth year as an undergraduate student in Engineering Physics at the University of Alberta. His research interests involve topics in optical and solid-state physics that are easily transferable to engineering applications. After completing his BSc, Torrey plans on pursuing graduate schooling in condensed matter physics.

Al Meldrum obtained a PhD in 1997 from the University of New Mexico. He then took a two-year postdoctoral fellowship at Oak Ridge National Laboratory, and subsequently signed on as an assistant professor at the University of Alberta. Now a full professor, his research interests are in silicon photonics, quantum dots, and sensing technologies.